 CMES, vol.22, no.3, pp.203-215, 2007

Lattice Boltzmann Method Simulation of Channel Flow with Square Pillars inside by the Field Synergy Principle

Cha'o-Kuang Chen[1], Shing-Cheng Chang[1] and Szu-Yu Sun[1]

Abstract: In this study, the channel flow is discussed by the LBM simulations. In the cases of channel with obstacles inside, the square pillars play the role of causing interruption within the fluid field, and hence change the direction of fluid flow. The recirculation region is formed behind the obstacles and influences the fluid passed through not only in the velocity field but also in the temperature field. Therefore, heat transfer is enhanced in local region.

The field synergy principle is applied in the research to demonstrate that the increased interruption within the fluid increases the synergistic level between the velocity field and temperature gradient field. As the intersection angle between the velocity vector and the temperature gradient vector is decreased by inserting square pillars to fluid field, the thermal efficiency of the channel is improved significantly.

Keyword: lattice Boltzmann method, field synergy principle, channel flow

1 Introduction

The lattice Boltzmann method (LBM) [Chen and Doolen (1998)] is a relatively new approach which utilizes parallel computing to study transport phenomena and has achieved considerable success in the computational fluid dynamics (CFD) simulations in the recent years. On the basis of the microscopic nature, the LBM treats the fluid on a statistical level and simulates the flow by tracking the evolution of one-particle phase space distribution rather than solving the macroscopic variables in the Navier-Stokes equations as the traditional CFD methods. The fundamental idea of the LBM is to construct simplified kinetic models which incorporate the essential physics of microscopic processes for the simulation of the flow with macroscopic averaged properties.

The lattice Boltzmann equation as a numerical scheme was first proposed by McNamara and Zanetti (1988). It simulates the movement and interaction of ensemble-average particle density distribution function of fluid by solving a velocity discrete Boltzmann equation and results in smooth macroscopic behaviors. Higuera and co-workers [Higuera and Jimenez (1989), Higuera, Succi and Benzi (1989)] introduced a linearized collision operator to simplify the scheme and eliminated the statistical noise. Current LBM adopt the simple relaxation Bhatnagar-Gross-Krook (BGK) model [Bhatnagar, Gross and Krook (1954)] for the collision operator. The lattice Boltzmann BGK (LBGK) model can be recovered to the Navier-Stokes equation successfully by the Chapman-Enskog expansion [Hou, Zou, Chen and Doolen (1995)], and therefore has been extensively applied to many kinds of the fluid research.

2D incompressible viscous flow [Nicolas and Bermudez (2004)] is a typical topic in the research of fluid flow and is studied by the LBM method in the recent years. By the coupled lattice Boltzmann method (LBM) and the discrete element method (DEM), Han, Feng and Owen (2007) investigated the irregular particle transport in turbulent flows. The current study investigates the flow and heat transfer phenomena of the 2D channel flow by the LBM simulation. In a channel with square pillars inside, the fluid flow would be separated by the pillars so the recirculation regions are formed in back of the pillars. Since the stream-

[1] Department of Mechanical Engineering, National Cheng-Kung University, Tainan, Taiwan, Republic of China. E-mail: ckchen@mail.ncku.edu.tw

lines of flow in the channel with pillars inside are more complex than that in the empty channel, the convective effect on heat transfer is also different.

To analyze the velocity and temperature fields in the channel flow, the field synergy principle [Guo, Li and Wang (1998), Wang, Li and Guo (1998)] is used in the study of the channel flow. Based on an analog between heat convection and heat conduction, Guo and co-workers studied the mechanism of convective heat transfer from a second look. They revealed that the convection term can be transformed into the form of dot product of velocity and temperature gradient, and the energy equation is integrated over the thermal boundary layer. The novel approaches of enhancing convective heat transfer involve improving the uniformity of velocity and temperature profiles as well as reducing the included angle between dimensionless velocity and temperature gradient vectors. Tao and co-workers (2002) called this concept the field synergy principle and extended from parabolic to elliptic fluid flow.

By the LBM simulation, the convective heat transfer phenomena of backward-facing step were studied in our previous work [Chen, Yen and Yang (2006)] with the field synergy principle. In this paper, the LBM is applied to simulate two-dimensional incompressible steady channel flow under low Reynolds number. The local influence on velocity and temperature fields is also analyzed by the field synergy principle.

2 Numerical Method

2.1 Lattice Boltzmann hydrodynamics model

In a fluid system, the evolution of the single-particle density distribution obeys the Boltzmann equation of BGK approximation:

$$\frac{\partial f}{\partial t}+\vec{v}\cdot\nabla f=-\frac{1}{\tau_\upsilon}(f-f^{eq}), \tag{1}$$

where $f(\vec{r},\vec{v},t)$ is the single-particle density distribution function, $\vec{v}$ is the microscopic velocity, and τ_υ is the relaxation time of the density distribution function towards the local equilibrium f^{eq} with respect to the Maxwell-Boltzmann equilibrium distribution function. The Boltzmann equation of BGK approximation can be transformed into the LBGK model by applied a lattice model with n dimensions and b lattice velocities, namely DnQb model [Qian, d'Humiéres and Lallemand (1992)], and described as

$$\frac{\partial f_\alpha}{\partial t}+\vec{e}_\alpha\cdot\nabla f_\alpha=-\frac{1}{\tau_\upsilon}(f_\alpha-f_\alpha^{eq}), \tag{2}$$

where $f_\alpha(\vec{r},t)$ and $\vec{e}_\alpha$ are the components of local distribution function and velocity respectively in the α direction of the lattice model. The discretized lattice Boltzmann equation is

$$f_\alpha(\vec{r}+\vec{e}_\alpha\Delta t,t+\Delta t)-f_\alpha(\vec{r},t) =-\frac{1}{\tau_\upsilon}[f_\alpha(\vec{r},t)-f_\alpha^{eq}(\vec{r},t)]. \tag{3}$$

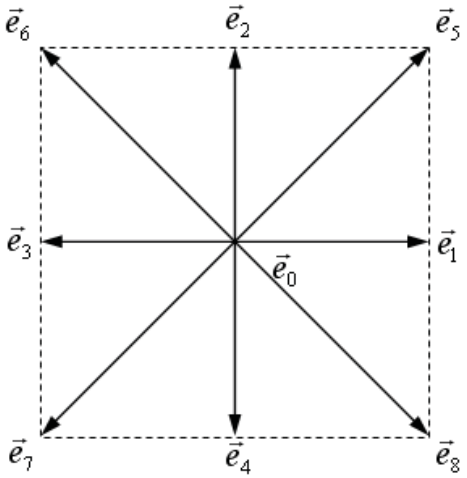

Figure 1: The D2Q9 model for LBM simulation.

In the present study, the D2Q9 lattice model is used to simulate the two-dimensional flow. The discrete velocity sets of this particular model are shown in Figure 1 and defined as

$$e_\alpha=\begin{cases}(0,0), & \alpha=0,\ \text{rest particle}\\ \left[\cos\frac{(\alpha-1)\pi}{2},\sin\frac{(\alpha-1)\pi}{2}\right]c, & \alpha=1,2,3,4\\ \left\{\cos\left[\frac{(\alpha-1)\pi}{2}+\frac{\pi}{4}\right],\sin\left[\frac{(\alpha-1)\pi}{2}+\frac{\pi}{4}\right]\right\}\sqrt{2}c, & \alpha=5,6,7,8\end{cases}, \tag{4}$$

where $c = \delta x/\delta t = \delta y/\delta t$ is the lattice streaming speed defined by the time stepδt and the grid spacing δx and δy. The equilibrium density distribution in LBGK model is given as

$$\begin{cases} f_\alpha^{eq}(\vec{r},t) = \frac{4}{9}\rho\left[1-\frac{3}{2}\vec{u}^2\right], & \alpha = 0 \\ f_\alpha^{eq}(\vec{r},t) = \frac{1}{9}\rho\left[1+\frac{3(\vec{e}_\alpha\cdot\vec{u})}{c^2}+\frac{9}{2}\frac{(\vec{e}_\alpha\cdot\vec{u})^2}{c^4}-\frac{3}{2}\frac{\vec{u}^2}{c^2}\right], & \alpha = 1,2,3,4 \\ f_\alpha^{eq}(\vec{r},t) = \frac{1}{36}\rho\left[1+\frac{3(\vec{e}_\alpha\cdot\vec{u})}{c^2}+\frac{9}{2}\frac{(\vec{e}_\alpha\cdot\vec{u})^2}{c^4}-\frac{3}{2}\frac{\vec{u}^2}{c^2}\right], & \alpha = 5,6,7,8 \end{cases}, \tag{5}$$

where $\vec{u}(\vec{r},t)$ is the velocity vector at the lattice node of position $\vec{r}$. In LBM simulation, the density distribution function f_α is obtained at each time step according to the evolution equation (3) with the equilibrium density distribution and the related relaxation time τ_υ. The macroscopic mass and momentum density are then calculated by

$$\rho = \sum_\alpha f_\alpha, \tag{6}$$

$$\rho\vec{u} = \sum_\alpha \vec{e}_\alpha f_\alpha. \tag{7}$$

By the Chapman-Enskog expansion [Hou, Zou, Chen and Doolen (1995)], the LBGK model can be recovered to the continuity equation and Navier-Stokes equation as below:

$$\partial_t\rho + \nabla\cdot(\rho\vec{u}) = 0, \tag{8}$$

$$\partial_t(\rho\vec{u}) + \nabla\cdot(\rho\vec{u}\vec{u}) = -\nabla p + \upsilon\left[\nabla^2(\rho\vec{u}) + \nabla(\nabla\cdot(\rho\vec{u}))\right], \tag{9}$$

where $p = c_s^2\rho$ is the pressure from the equation of state for the ideal gas and $c_s = c/\sqrt{3}$ is the sound speed. The kinematic viscosity is given by

$$\upsilon = \frac{2\tau_\upsilon - 1}{6}\frac{(\delta x)^2}{\delta t}. \tag{10}$$

The incompressible limit of fluid flow is approached with the low Mach number assumption, i.e. $M \ll 1$, where $M = \vec{u}/c_s$. The incompressible continuity equation and Navier-Stokes equation are expressed as

$$\nabla\cdot\vec{u} = 0, \tag{11}$$

$$\partial_t\vec{u} + \vec{u}\cdot\nabla\vec{u} = -\frac{\nabla p}{\rho} + \upsilon\nabla^2\vec{u}. \tag{12}$$

2.2 Lattice Boltzmann thermal model

The thermal model for LBM simulation used in this study is proposed by Peng, Shu and Chew (2003), which is the simplified thermal energy distribution model of He, Chen and Doolen (1998). In the work of He, Chen and Doolen, the internal energy distribution function was introduced to simulate the temperature field for solving real thermal problems. However, the model contains one complicated gradient operator term in the evolution equation for the temperature, and hence the simplicity property of the LBM has been lost. Another disadvantage for this model is that the viscosity is involved not only in the momentum equation but also in the energy equation. To keep the consistent of viscosity in the governing equations for the thermal energy distribution model and avoid the implicitness of the schemes, new additional variables for the thermal energy distribution function are used. The detail of the thermal lattice Boltzmann model is given by He, Chen and Doolen (1998) and will not be shown here.

For incompressible flow, Peng, Shu and Chew indicated that the compression work done by the pressure and the viscous heat dissipation can be neglected, so the gradient term can be dropped out in the model of He, Chen and Doolen. The evolution model of simplified thermal energy distribution for LBM simulation is expressed as

$$g_\alpha(\vec{r}+\vec{e}_\alpha\Delta t, t+\Delta t) - g_\alpha(\vec{r},t) = -\frac{1}{\tau_c}\left[g_\alpha(\vec{r},t) - g_\alpha^{eq}(\vec{r},t)\right], \tag{13}$$

where τ_c is the relaxation time of the internal energy distribution function, $g_\alpha(\vec{r},t)$. The equilib-

rium energy distribution function is given as

$$\begin{cases} g_\alpha^{eq}(\vec{r},t) = -\frac{2}{3}\rho\varepsilon\frac{\vec{u}^2}{c^2}, & \alpha = 0 \\ g_\alpha^{eq}(\vec{r},t) = \frac{1}{9}\rho\varepsilon\left[\frac{3}{2}+\frac{3}{2}\frac{(\vec{e}_\alpha\cdot\vec{u})}{c^2}+\frac{9}{2}\frac{(\vec{e}_\alpha\cdot\vec{u})^2}{c^4}-\frac{3}{2}\frac{\vec{u}^2}{c^2}\right], & \alpha = 1,2,3,4 \\ g_\alpha^{eq}(\vec{r},t) = \frac{1}{36}\rho\varepsilon\left[3+\frac{6(\vec{e}_\alpha\cdot\vec{u})}{c^2}+\frac{9}{2}\frac{(\vec{e}_\alpha\cdot\vec{u})^2}{c^4}-\frac{3}{2}\frac{\vec{u}^2}{c^2}\right], & \alpha = 5,6,7,8 \end{cases} \quad (14)$$

where ε is calculated according to equation (13) by

$$\rho\varepsilon = \sum_\alpha g_\alpha. \quad (15)$$

Then the macroscopic temperature can be obtained by the relation of $\varepsilon = DRT/2$, in which R is the gas constant and D is the dimension. Peng, Shu and Chew (2003) showed that the macroscopic energy equation can be derived from the evolution equation (13) for the thermal energy distribution function by the Chapman-Enskog expansion, and expressed as

$$\partial_t(\rho\varepsilon) + \nabla\cdot(\rho\vec{u}\varepsilon) = \chi\nabla^2(\rho\varepsilon), \quad (16)$$

where the diffusivity χ is determined by

$$\chi = \frac{2}{3}\left(\tau_c - \frac{1}{2}\right)c^2\delta t. \quad (17)$$

Comparing with the model of He, Chen and Doolen, the simplified thermal energy distribution model by Peng, Shu and Chew does not use the new variables that would complicate the calculation process. Otherwise, it does not include the complex gradient term in the evolution equation and keeps the same simple form as the isothermal LBM. Since the variables for the evolution equations and the boundary conditions are consistent, the boundary condition is very easy to implement for this model, e.g. the bounce-back rule of the non-equilibrium distribution function is adoptable.

2.3 Simulation model

Figure 2 showed the simulation model of the channel flow without any build-in obstacles. This case is denoted as case (1) in contrast to the cases with square pillars inside the channel. The lattice streaming speed, $c = 1$, is applied in all simulation model for the dimensionless uniform grids $\delta x = \delta y = 1$ and time step $\delta t = 1$. The boundary conditions for the inlet, outlet, and the wall in the case (1) are detailed as follows.

(a) The inlet (boundary $\overline{ab}$):

At the entrance of the channel, a uniform velocity flow is specified. The velocity is chosen to be lower than 10% of the speed of sound for the LBM simulation to avoid significant compressibility effects which are known to be increased with the square of the Mach number. By the method of pressure and velocity boundary conditions proposed by Zou and He (1997) for LBM, the equilibrium density distribution function is computed from the given velocity and imposed at the first lattice column. In the inlet, the unknown components of mass density distribution function in the evolution of time step are f_1, f_5, and f_8. These can be obtained by the mass and momentum equations, i.e. equation (6) and (7), as the form of

$$f_1 + f_5 + f_8 = \rho - (f_0 + f_2 + f_3 + f_4 + f_6 + f_7), \quad (18)$$

$$f_1 + f_5 + f_8 = \rho u_x + (f_3 + f_6 + f_7), \quad (19)$$

$$f_5 - f_8 = \rho u_y - (f_2 - f_4 + f_6 - f_7), \quad (20)$$

with f_1, f_5, and f_8 left. In the equations $\vec{u} = (u_x, u_y)$ is the given velocity of the inlet. Note that the local density ρ is not a given value and can be calculated by

$$\rho = \frac{1}{1-u_x}\left[f_0 + f_2 + f_4 + 2(f_3 + f_6 + f_7)\right], \quad (21)$$

according to equation (18) and (19).

To solve the unknowns, the bounce-back rule of the non-equilibrium distribution is introduced for the term perpendicular to the boundary, i.e.

$$f_1 - f_1^{eq} = f_3 - f_3^{eq}, \quad (22)$$

or

$$f_1 = f_3 + \frac{2}{3}\rho u_x, \quad (23)$$

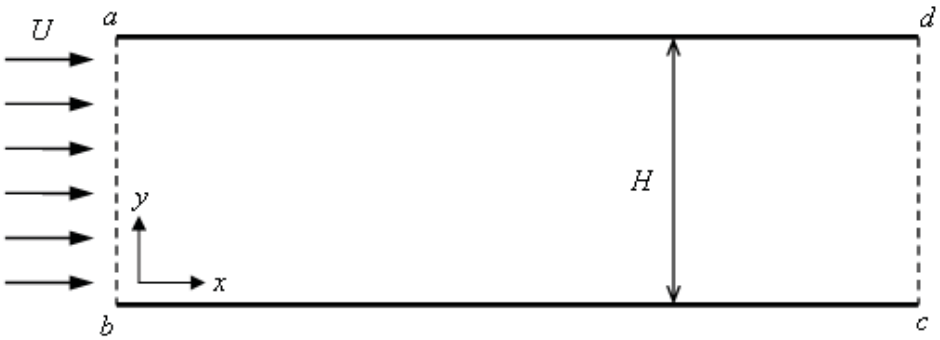

Figure 2: The simulation case (1) of channel flow without any build-in obstacles.

with corresponding to the equilibrium density distribution in equation (5). Then f_5 and f_8 can be given by solving the mass and momentum equations as

$$f_5 = f_7 - \frac{1}{2}(f_2 - f_4) + \frac{1}{6}\rho u_x + \frac{1}{2}\rho u_y, \tag{24}$$

$$f_8 = f_6 + \frac{1}{2}(f_2 - f_4) + \frac{1}{6}\rho u_x - \frac{1}{2}\rho u_y. \tag{25}$$

In the research of heat transfer phenomena, the Dirichlet type condition is applied on the inlet boundary with a given temperature, T_{in}. The thermal energy distribution function at the entrance satisfied:

$$g_\alpha^{neq} - e_\alpha^2 f_\alpha^{neq} = -\left(g_\beta^{neq} - e_\beta^2 f_\beta^{neq}\right), \tag{26}$$

where e_α and e_β have opposite directions.

(b) The outlet (boundary $\overline{cd}$):

At the outlet a fixed pressure is imposed in terms of the equilibrium distribution function. The pressure boundary condition is also implemented by the method of Zou and He (1997) with the same procedure as the velocity boundary above. The Dirichlet type condition is also applied on the outlet by a given temperature, $T_{out} < T_{in}$.

(c) The fixed wall (boundary $\overline{ad}$ and $\overline{bc}$):

The bounce-back rule of the non-equilibrium distribution applied in the inlet and outlet boundary is also used for no slip boundary condition on the fixed wall. Additionally, a given temperature, $T_w = T_{out} < T_{in}$, is applied on the wall for the Dirichlet type condition.

By the implementation of boundary conditions, the flow and thermal field in the channel of case (1) is discussed in the later section. In the simulation case (2), a build-in square pillar of the size and position shown in Figure 3 is located in the channel. The velocity and thermal boundary conditions of the inlet, outlet, and fixed wall are the same as in the case (1). To eliminate the effect of other factors, the inserted obstacle is particularly assumed to be thermally isolated from other heat source so that the only function of that is to introduce interruption within the fluid. For the Neumann type condition, i.e. adiabatic or constant heat flux condition, it was transferred to the Dirichlet type condition through the conventional second-order finite difference approximation to get the temperature on the boundary [Shu, Peng and Chew (2002)]. When the temperature gradient is given, the temperature on the boundary can be calculated by

$$\left.\frac{\partial T}{\partial y}\right|_{x,1} = \frac{-3T_{x,1} + 4T_{x,2} - T_{x,3}}{2\Delta y}. \tag{27}$$

No matter the adiabatic or constant heat flux boundary condition we choose, through the equation (27) we can get the corresponding Dirichlet type boundary condition.

The effect of a build-in obstacle on the flow and temperature field in the channel is investigated by comparing with case (1) and (2). In addition, another square pillar is inserted at the back of the first one with the same size in case (3) to further study the enhancement of convective heat transfer by obstacles inside the channel. The related position of the obstacles is shown in Figure 4.

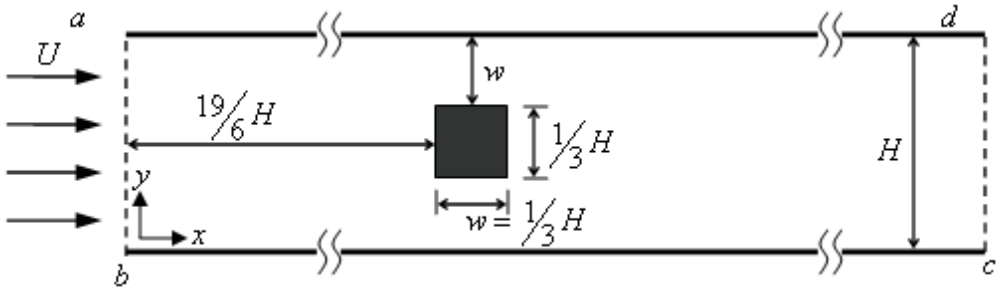

Figure 3: The simulation case (2) of channel flow with a square pillar inside.

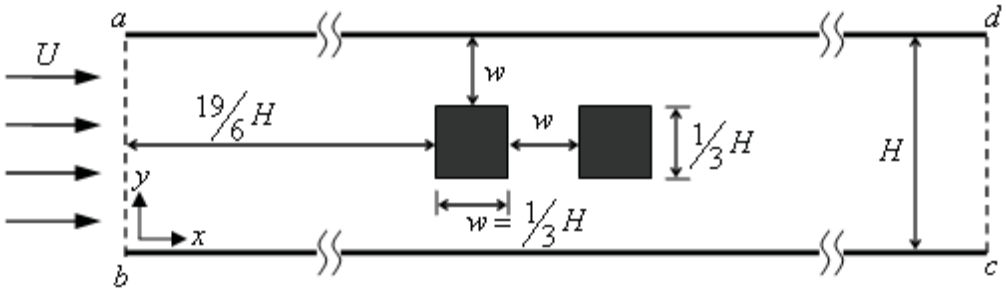

Figure 4: The simulation case (3) of channel flow with two square pillars inside.

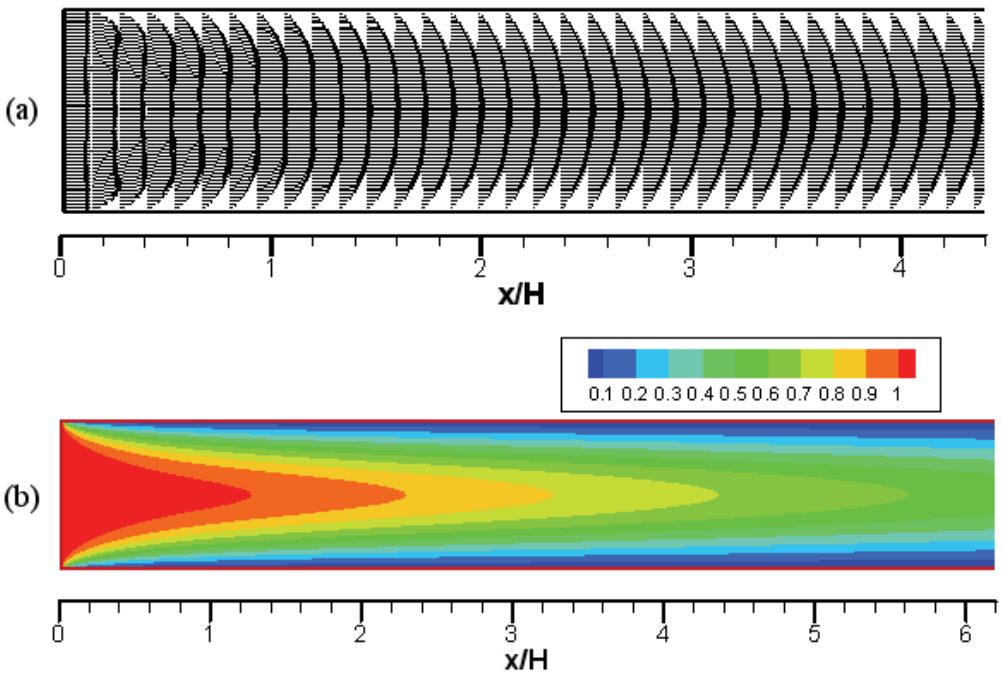

Figure 5: (a) Velocity profiles and (b) temperature distribution of case (1) with Re=90 and Pr=0.7.

In each run, the following inequality is used as the criterion of convergence,

$$\frac{\sum_{i,j}\left\|\vec{u}(r_{i,j},t+\delta t)-\vec{u}(r_{i,j},t)\right\|}{\sum_{i,j}\left\|\vec{u}(r_{i,j},t)\right\|}\leq 1.0\times 10^{-6}, \tag{28}$$

$$\frac{\sum_{i,j}\left\|\varepsilon(r_{i,j},t+\delta t)-\varepsilon(r_{i,j},t)\right\|}{\sum_{i,j}\left\|\varepsilon(r_{i,j},t)\right\|}\leq 1.0\times 10^{-6}. \tag{29}$$

3 Results and Discussion

3.1 Analysis of the channel flow without obstacles

In a channel, the phenomena of heat fluid flowing to an outlet of low temperature are investigated. The temperature of the wall in the channel is considered to be the same as the outlet, i.e. the cooling wall is adopted in the simulation. By applying a uniform velocity in the entrance, the velocity profiles in the channel are changed from a plug-like form to a full developed curve of a parabolic form due to the effect of viscosity, as shown in Figure 5(a). The Reynolds number, Re=90, and the Prandtl number, Pr=0.7 are specified in this case. In the LBM simulation, the Reynolds number is given by

$$\mathrm{Re}=\frac{UH}{\nu}, \tag{30}$$

and the Prandtl number is defined as the ratio of momentum diffusivity to heat diffusivity by

$$\mathrm{Pr}=\frac{\nu}{\chi}=\frac{\tau_\nu-0.5}{2(\tau_c-0.5)}. \tag{31}$$

relating to the relaxation time of the density distribution function, τ_ν, and of the internal energy distribution function, τ_c.

Because of the temperature difference between the hot entering fluid and the cooling wall, the thermal boundary layer is formed by the effects of convective and conductive heat transfer. The temperature distribution of this case is shown in Figure 5(b), in which the temperature values are presented as a dimensionless form of $T^*=(T-T_w)/(T_{in}-T_w)$. Figure 5(b) reveals that as the distance of fluid from the inlet increases, the local temperature in the channel decreases because of the thermal boundary effect. Actually, an exponential-type decay relation is observed in Figure 6 of the diagram of Nusselt number, Nu, in the bottom wall related to x direction.

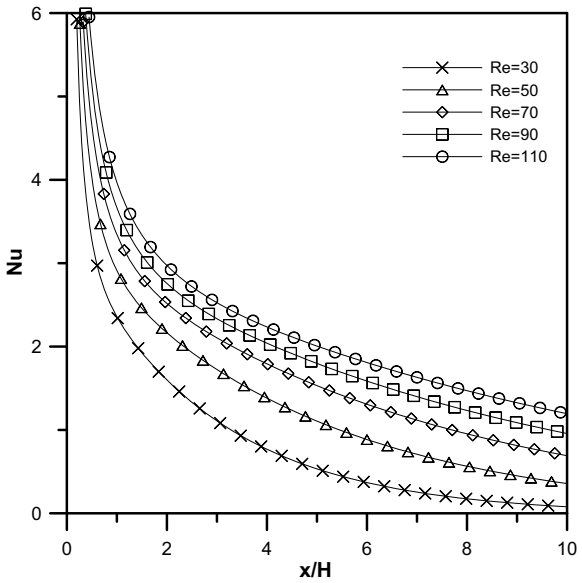

Figure 6: Influence of Reynolds number on Nusselt number for case (1) with Pr=0.7.

The influence of different Reynolds number of Re=30, 50, 70, 90, and 110 on Nusselt number is also displayed in Figure 6. The Prandtl number is fixed to Pr=0.7 here. It reveals that the convective effect on heat transfer is enhanced as the Reynolds number is increased. Obviously, heat can be further transported in high Reynolds number, i.e. higher temperature can be observed downstream in the case of Re=110 than of Re=30 and 70, as shown in Figure 7. By choosing Pr=0.4, 0.7, 1.0 and Re=70, the influence of the Prandtl number on the temperature distribution is investigated and the diagram of Nusselt number variation is shown in Figure 8. The case of high Prandtl number is found to be with good convective effect because of the powerful momentum diffusivity. The related temperature contours of the three cases are shown in Figure 9.

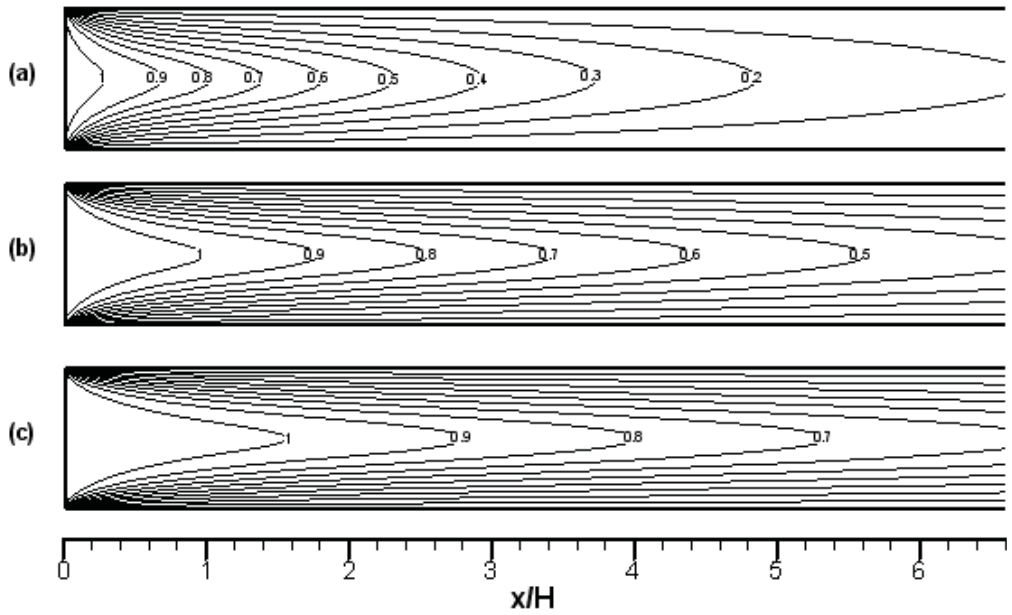

Figure 7: Temperature contours of case (1) with Pr=0.7 and (a) Re=30, (b) 70 and (c) Re=110.

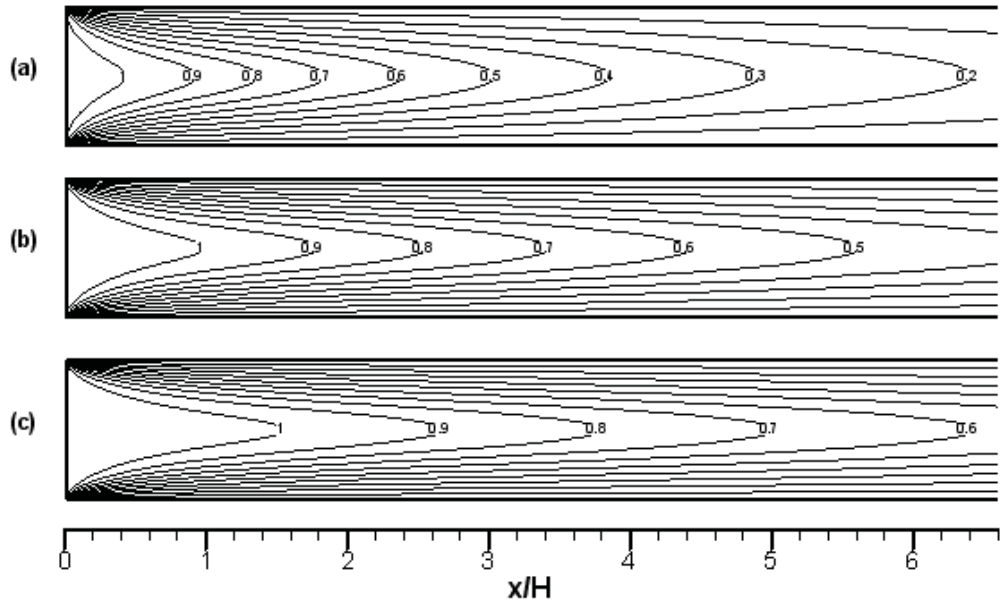

Figure 9: Temperature contours of case (1) with Re=70 and (a) Pr=0.4, (b) Pr=0.7 and (c) Pr=1.0.

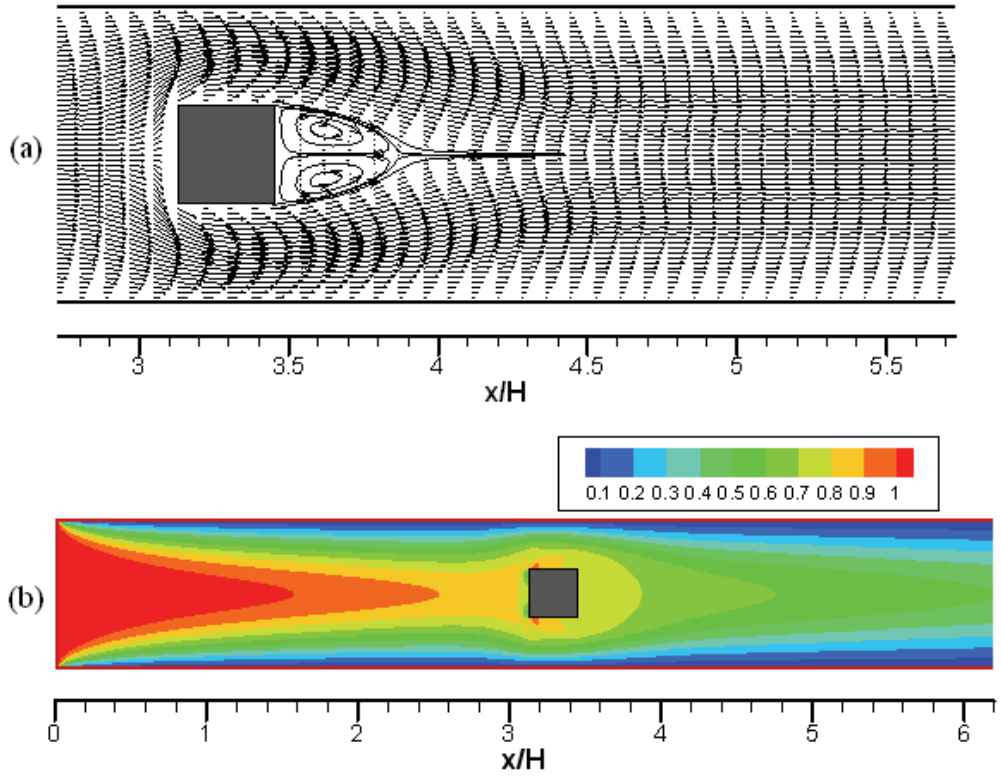

Figure 10: (a) Velocity profiles and (b) temperature distribution of case (2) with Re=90.

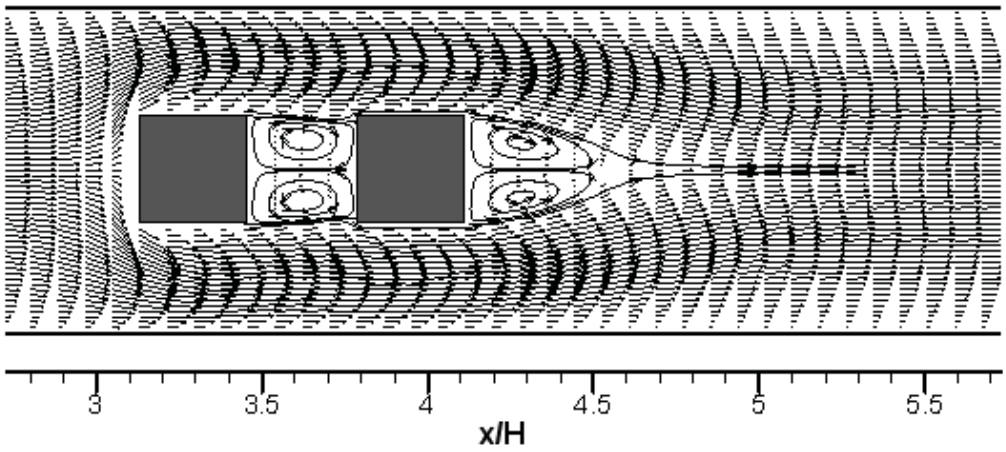

Figure 12: Velocity profiles of case (3) with Re=90.

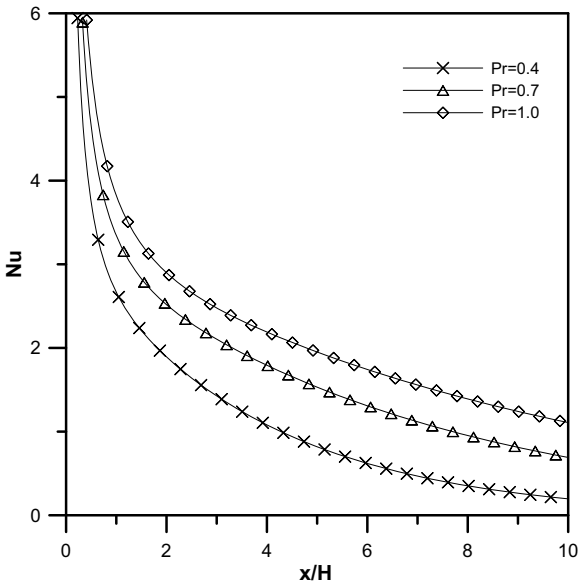

Figure 8: Influence of Prandtl number on Nusselt number for case (1) with Re=70.

3.2 Analysis of the channel flow with obstacles

In the analysis of the channel flow with obstacles, the effect of the Prandtl number on heat transfer is no more emphasized, and an identical Prandtl number, Pr=0.7, is used in the simulation cases here. By inserting a square pillar located within the channel center, the entering fluid flows through the obstacle via a narrowed sub-channel of the size with $2/3$ channel width with raising velocity. Figure 10 shows the velocity profiles and temperature distribution of case (2) with Re=90. It shows that flow separation phenomena appear near the back corner and a stable recirculation region is formed behind the obstacle with two symmetrical eddies. It is found that the size of recirculation region would be enlarged as the Reynolds number is increased. The simulation results indicate that heat of fluid is transferred accompanying with the mass diffusion through the same path. Comparing with Figure 5(b) and Figure 10(b), it presents that energy transportation is hindered by the adiabatic obstacle so that the temperature behind the obstacle is lower in the case (2) than that in the case (1) in the same section. Nevertheless, temperature in the section between the inlet and the obstacle in the case (2) is higher than that in the case (1) due to the heat rebounding.

Inspecting the diagram of Nusselt number in case (2) with different Reynolds number, as shown in Figure 11, a distinct peak of the decay curve appears at the location in front of the obstacle in the cases of Re=30, 50, and 70. When the Reynolds number is raised over Re=90, another peak of the position in the section of recirculation region is observed. The first peak is due to the influence of channel narrowing. The fluid is accelerated with y-component velocity arisen when flowing through the obstacle. This enhances the convective effect and causes the energy density distribution to be increased ahead of the obstacle. The second peak is caused by the eddy, which is large enough to contribute to convective effect in the cases of high Reynolds number. In the low Re cases in Figure 11, the enhancement of heat transfer by recirculation region is not obvious.

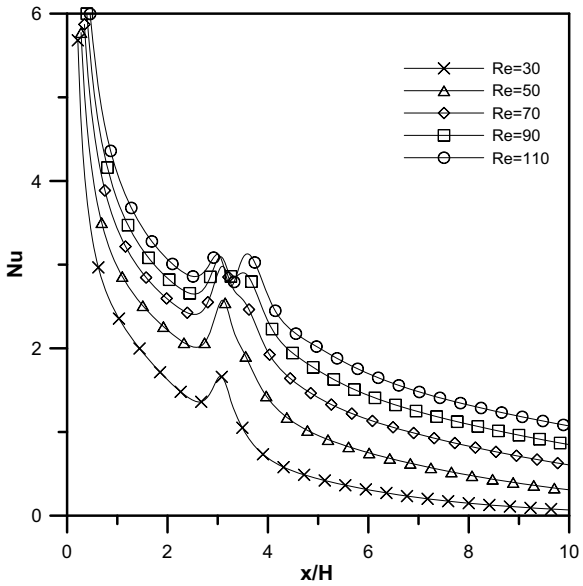

Figure 11: Influence of Reynolds number on Nusselt number for case (2).

To further investigate the influence of multi-obstacles inside the channel on the convective heat transfer, two square pillars are put in the channel with positions as mentioned above in the case (3). The velocity profiles in this case are displayed in Figure 12. It is observed that the recirculation regions are generated both between the

two obstacles and after the second obstacle. In Figure 12, it is deserved to be mentioned that although the section among the obstacles has the same width as the unhindered channel, the width of flow path is not extended apparently when the fluid flows through the section. This is because the obstacle-like eddy in the region keeps on narrowing the channel. In other words, this eddy and the obstacles can be viewed as a combined rectangular object. The effect of combination is important not only on velocity field but also temperature field. Figure 13 showed the diagram of Nusselt number for the case (3). It is found that the peak caused by the second pillar is not distinct as that by the first one in all cases of different Reynolds number. The results show that the influence of channel narrowing by the second obstacle is not overemphasized as by the first obstacle. However, the effect of big eddy on enhancing convective heat transfer is still presented in the case of Re=110. Two additional peaks are found in the curve of Re=110 in Figure 13.

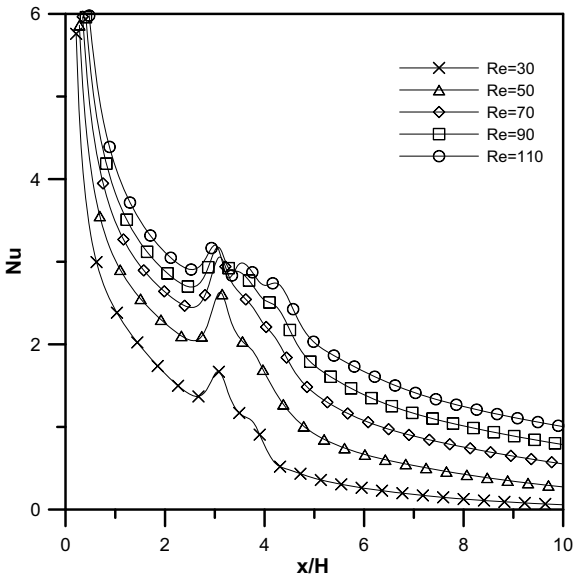

Figure 13: Influence of Reynolds number on Nusselt number for case (3).

3.3 *Demonstration for enhancing convective heat transfer by the field synergy principle*

The steady state 2D incompressible energy equation of fluid flow and heat transfer over a channel is

$$\rho c_p \left(u\frac{\partial T}{\partial x} + \upsilon\frac{\partial T}{\partial y} \right) = \frac{\partial}{\partial x}\left(k\frac{\partial T}{\partial x} \right) + \frac{\partial}{\partial y}\left(k\frac{\partial T}{\partial y} \right). \quad (32)$$

In this elliptic fluid flow, the definition of the Int value is defined as [Tao, Guo and Wang (2002)]

$$Int = \int_\Omega \rho c_p (\vec{V}\cdot\nabla T) dxdy, \quad (33)$$

where

$$\vec{V}\cdot\nabla T = \left|\vec{V}\right| |\nabla T| \cos\theta. \quad (34)$$

By raising the Int number of the integral of the convection term, i.e. heat source, over the computation domain, the convective heat transfer can be enhanced. From the field synergy principle's point of view, the average intersection angle, θ_m, between the velocity vector and the temperature gradient in the computation domain is as important as the Reynolds number and the Prandtl number for enlarging the Int number. That is to say, the better synergy of the flow and temperature field leads to the better thermal efficiency.

There are three mechanisms to enhance single phase convective heat transfer, including increasing the flow interruption, decreasing the thermal boundary layer, and increasing the velocity gradient near a solid wall [Guo, Li and Wang (1998)]. By inserting obstacles inside the channel, the fluid flow is interrupted and the thermal performance of the channel is enhanced. The influence of Reynolds number on average Nusselt number in the channel of case (1), (2), and (3) is shown in Figure 14. The thermal efficiency of the channel with two obstacles is found to be better than the other cases, especially in high Reynolds number case. Figure 15 shows the dimensionless Int number of the three simulation cases about the different Reynolds number. The trend of Int number is consistency with the result of Figure 14. Larger Int number is obtained in the case (3) than in the other cases, i.e. the thermal efficiency of the flow is better by inserting two square pillars.

The variation of average intersection angle is shown in Figure 16 to inspect the synergy of the

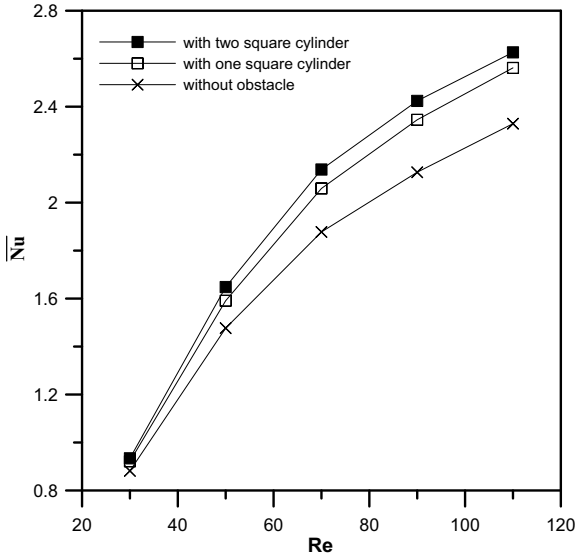

Figure 14: Effect of Reynolds number on average Nusselt number in the channel.

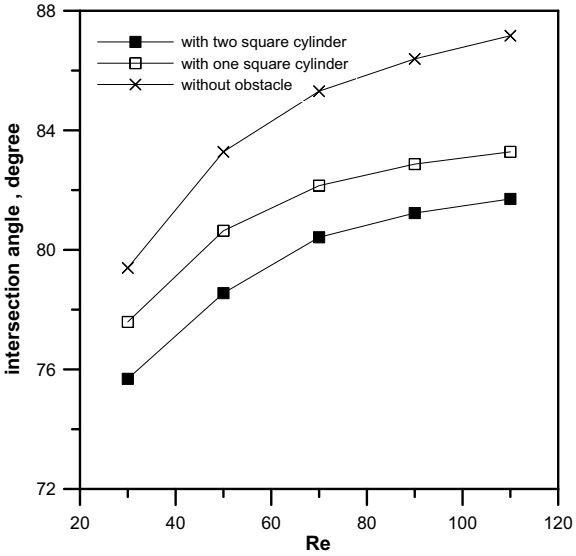

Figure 16: Effect of Reynolds number on average intersection angle.

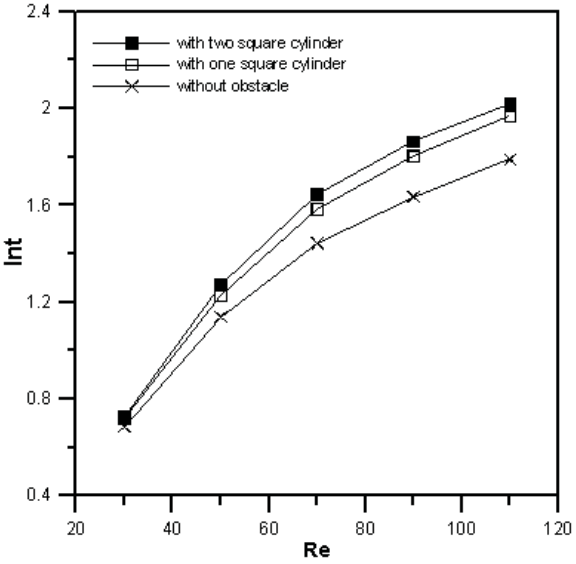

Figure 15: Effect of Reynolds number on dimensionless Int number.

velocity and the temperature field of the flow. If the local value of θ is greater than 90°, its value is taken as $(180^\circ - \theta)$ when added to the summation of the intersection angle [Tao, He, Wang, Qu and Song (2002)]. In the condition of Re=110, the average intersection angle of case (1) is 3.88° and 5.46° smaller than that in the case (2) and (3) respectively. It shows that by inserting obstacles in the channel, the intersection angle is decreased, i.e. a better synergy is attained, so that the Int value or the thermal efficiency is increased.

4 Conclusions

The lattice Boltzmann method is applied to simulate the two-dimensional incompressible steady flow in a channel with or without obstacles inside. The D2Q9 lattice model [Qian, d'Humiéres and Lallemand (1992)] for density distribution function of fluid and the thermal lattice model by Peng, Shu and Chew (2003) for internal energy distribution function are adopted in the LBM simulation. In the case of channel with build-in square pillars, the fluid is interrupted as flowing through the obstacles, and the recirculation regions are formed behind the obstacles. As an obstacle-like body, the eddy affected not only the velocity profiles of the fluid passed through, but also the heat transfer efficiency of the local flow region.

In the statement of the field synergy principle, the thermal efficiency of the parabolic or elliptic fluid flow can be enhanced by increasing the synergistic level of the flow field. To study the heat transfer efficiency of the channel flow, the integral of heat source term and the average intersection an-

gle are calculated in the simulation. The results presented that the thermal efficiency is improved significantly by inserting obstacles inside a channel, i.e. the average Nusselt number or the Int number is increased as the average intersection angle is decreased. By the analysis of the field synergy principle, the results showed that there is still many ways to enhance the heat transfer efficiency in a channel flow.

Acknowledgement: This study acknowledges the support provided to this research by the National Science Council of Republic of China under Grant No. NSC-94-2212-E-006-020.

References

Bhatnagar, P.L.; Gross, E.P.; Krook, M. (1954): A model for collision process in gases. I. Small amplitude processes in charged and neutral one component system. *Phys. Rev.*, vol. 94, pp. 511-521.

Chen, S.; Doolen, G. D. (1998): Lattice Boltzmann method for fluid flows. *Annu. Rev. Fluid Mech.*, vol. 30, pp. 329-364.

Chen, C. K.; Yen, T. S.; Yang, Y. T. (2006): Lattice Boltzmann method simulation of backward-facing step on convective heat transfer with field synergy principle. *Int. J. Heat Mass Transfer*, vol. 49, pp. 1195-1204.

Guo, Z.Y.; Li, D.Y.; Wang, B.X. (1998): A novel concept for convective heat transfer enhancement. *Int. J. Heat Mass Transfer*, vol. 41, pp. 2221-2225.

Han, K.; Feng, Y. T., Owen, D. R. J. (2007): Numerical Simulations of Irregular Particle Transport in Turbulent Flows Using Coupled LBM-DEM. *CMES: Computer Modeling in Engineering & Sciences*, Vol. 18, No. 2, pp. 87-100.

He, X.; Chen, S.; Doolen, G.D. (1998): A novel thermal model for the lattice Boltzmann method in incompressible limit. *J. Comput. Phys.*, vol. 146, pp. 282-300. **Higuera, F.; Jimenez, J.** (1989): Boltzmann approach to lattice gas simulations. *Europhys. Lett.*, vol. 9, pp. 663-668.

Higuera, F.; Succi, S.; Benzi, R. (1989): Lattices gas dynamics with enhanced collisions. *Europhys. Lett.*, vol. 9, pp. 345-349.

Hou, S.; Zou, Q.; Chen, S.; Doolen, G. (1995): A.C. Cogley, Simulation of cavity flow by the lattice Boltzmann method. *J. Comput. Phys.*, vol. 118, pp. 329-347.

McNamara, G.; Zanetti, G. (1988): Use of the Boltzmann equation to simulate Lattice-Gas Automata. *Phys. Rev. Lett.*, vol. 61, pp. 2332-2335.

Nicolas, A.; Bermudez, B. (2004): 2D Incompressible Viscous Flows atModerate and High Reynolds Numbers. *CMES: Computer Modeling in Engineering & Sciences*, Vol. 6, No. 5, pp. 441-451.

Peng, Y.; Shu, C.; Chew, Y.T. (2003): Simplified thermal lattice Boltzmann model for incompressible thermal flows. *Phys. Rev. E.*, vol. 68, pp. 026701.

Qian, Y. H.; d'Humiéres, D.; Lallemand, P. (1992): Lattice BGK models for Navier-Stokes equation. *Europhy. Lett.*, vol. 17, pp. 479-484.

Wang, S.; Li, Z.X.; Guo, Z.Y. (1998): Novel concept and device of heat transfer augmentation. in: *Proc. of 11th IHTC*, vol. 5, pp. 405-408.

Shu, C.; Peng, Y.; Chew, Y.T. (2002): Simulation of Natural Convection in a Square Cavity by Taylor series expansion and Least square-based Lattice Boltzmann Method. *Int. J. Modern Phys. C*, vol. 13, pp. 1399-1414.

Tao, W.Q.; Guo, Z.Y.; Wang, B.X. (2002): Field synergy principle for enhancing convective heat transfer–its extension and numerical verifications. *Int. J. Heat Mass Transfer*, vol. 45, pp.3849-3856.

Tao, W.Q.; He, Y.L.; Wang, Q.W.; Qu, Z.G.; Song, F.Q. (2002): A unified analysis on enhancing single phase convective heat transfer with field synergy principle. *Int. J. Heat Mass Transfer*, vol. 45, pp. 4871-4879.

Zou, Q.; He, X. (1997): On pressure and velocity boundary conditions for the lattice Boltzmann BGK model. *Phys. Fluids*, vol. 9, pp. 1591-1598.